
STRUCTURE NOTE

Crystal Structure of 5'-Methylthioadenosine Nucleosidase From *Arabidopsis thaliana* at 1.5-Å Resolution

Eun Young Park,¹ Seung-Ick Oh,¹ Min Jung Nam,² Jeong Sheop Shin,¹ Kyung-Nam Kim,² and Hyun Kyu Song^{1*}

¹School of Life Sciences and Biotechnology, Korea University, Seoul 136-701, Korea

²Department of Molecular Biology, Sejong University, Seoul 143-747, Korea

Introduction. Methylthioadenosine (5'-deoxy-5'-methylthioadenosine; adenine-9-β-D-(5'-deoxy-5'-methylthio)-ribofuranoside, MTA) is an important metabolite in all living organisms. MTA is involved in methionine (Met) and S-adenosyl-Met (AdoMet) recycling, polyamine biosynthesis, and bacterial quorum sensing.¹ The metabolism of MTA is clearly characterized by extensive studies on the identification and characterization of enzymes in reaction pathways and the examination of reaction intermediates, particularly in bacterial systems.² Several gene products in the pathways are attractive targets for antibiotics in prokaryotes and have been demonstrated as potential therapeutics in mammals.³ The MTA cycle has also been studied extensively in plant because of the synthesis of ethylene and polyamines, where the maintenance of their levels is important in plant physiology.⁴ Many genes involved in the MTA cycle in plant have also been isolated and characterized.^{5–7} One of the key enzymes in this cycle is 5'-methylthioadenosine nucleosidase (MTAN). MTAN (EC 3.2.2.16) is an enzyme that irreversibly cleaves the ribosidic bond of MTA to produce 5'-methylthioribose (MTR) and adenine. In bacteria and plants, MTR kinase subsequently phosphorylates the C-1 hydroxyl group of the ribose moiety of MTR to yield MTR-1-phosphate, while MTA phosphorylase (MTAP) is known to carry out both functions in a single step in mammals.^{1,8} Mammals utilize two separate enzymes, MTAP and S-adenosylhomocysteine (AdoHcy) hydrolase, to catabolize MTA and AdoHcy, whereas bacteria use a dual substrate-specific MTA/AdoHcy nucleosidase. Plants hydrolyze MTA and AdoHcy differently. The biochemical characterization of MTAN from *Lupinus leteus* and *Pisum sativum* seeds has indicated an ability to discriminate between the analogs with and without an α-amino group at the 5'-alkylthiomoiety.^{9,10} Plants utilize MTAN and AdoHcy hydrolase separately to cleave the ribosidic bond of MTA and AdoHcy, respectively. Thus, the AdoHcy hydrolase activity in plant has been lost compared with the bacterial enzyme. Sequence alignment of *E. coli* MTA/AdoHcy nucleosidase (EcMTAN) and plant MTAN shows a high degree of sequence conservation among the residues in the active site, despite limited overall sequence identity.⁸ Extensive biochemical and

structural studies on EcMTAN have provided a wealth of information regarding the catalytic mechanism, specific interactions with MTA, and conformational changes for the enzymatic reaction.¹¹ No structural information is available, however, on a plant MTAN, a similar enzyme with different specificity. To gain insight into the structural basis of the differences in substrate specificity, we have determined the high-resolution structure of MTAN from *Arabidopsis thaliana* (AtMTAN).

Materials and Methods. The full-length MTAN gene (AT4G38800) from *Arabidopsis thaliana* was cloned using standard polymerase chain reaction techniques. The gene was flanked by EcoRI and Sall restriction enzyme sites, and the fragments were ligated into a pGEX-4T-3 expression vector. The integrity of the plasmids that were produced was verified by DNA sequencing and the plasmids were then transformed into BL21(DE3)RIL cells. Expression of the MTAN was induced by the addition of 1 mM IPTG at OD (600 nm) = 0.6. After 20-h induction at 22°C, the cells were harvested by centrifugation and kept frozen at –80°C till further use. The cell pellets were resuspended in ice-cold 1× PBS in the presence of 1 mM PMSF and subsequently disrupted by ultrasonication. The proteins were applied to a glutathione column as the first step and eluents from the column were subjected to SDS-PAGE followed by visualization with Coomassie blue staining.

Abbreviations: AdoHcy, S-adenosylhomocysteine; AtMTAN, *Arabidopsis thaliana* MTAN; EcMTAN, *E. coli* MTA/AdoHcy nucleosidase; MAD, multiwavelength anomalous dispersion; MTAN, 5'-methylthioadenosine nucleosidase; MTAP, 5'-methylthioadenosine phosphorylase; MTR, 5'-methylthioribose; SeMet, selenomethionine.

Grant sponsor: BioGreen 21 Program, Rural Development Administration, Republic of Korea, Plant Signaling Network Research Center, Korea Science and Engineering Foundation, Seoul R&BD Program.

*Correspondence to: Hyun Kyu Song, School of Life Sciences and Biotechnology, Korea University, Anam-dong, Seongbuk-gu, Seoul 136-701, Korea. E-mail: hksong@korea.ac.kr

Received 21 April 2006; Accepted 6 June 2006

Published online 14 August 2006 in Wiley InterScience (www.interscience.wiley.com). DOI: 10.1002/prot.21120

TABLE I. Data Collection and Refinement Statistics

	Native	Hg-derivative (MAD)				SeMet (MAD)		
<u>Data collection</u>								
Space group	P2 ₁	P2 ₁				P2 ₁		
	Cell dimension							
<i>a</i> , <i>b</i> , <i>c</i> (Å)	40.54, 126.59, 45.79		40.89, 126.60, 45.80			40.13, 126.42, 45.53		
α , β , γ (°)	90.0, 104.98, 90.0		90.0, 104.35, 90.0			90.0, 105.66, 90.0		
X-ray sources ^a	NW12, PF		4A, PAL			4A, PAL		
		Remote	Edge 1	Edge 2	Peak	Remote	Edge	Peak
Wavelength (Å)	1.0000	0.9918	1.0064	1.0084	1.0087	0.9500	0.9795	0.9797
Resolution (Å) ^b	1.5 (1.55)	2.5 (2.59)	2.5 (2.59)	2.5 (2.59)	2.5 (2.59)	2.5 (2.59)	2.5 (2.59)	2.5 (2.59)
<i>R</i> _{merge} (%) ^c	5.0	8.1	7.8	8.0	9.3	8.2	8.7	9.7
Total reflections	196,061	101,659	97,472	97,820	101,843	114,502	110,197	112,191
Unique reflections	67,182	15,539	14,980	14,981	15,072	15,467	15,501	15,327
Completeness (%)	94.0	99.8	94.8	94.7	95.4	99.9	99.7	99.4
FOM ^d					0.59			
<u>Refinement</u>								
Resolution range (Å)	50.0–1.5							
Reflections used	64,982							
<i>R</i> _{work} / <i>R</i> _{free} (%) ^e	19.8/22.4							
Number of atoms								
Protein	3,678							
Water/adenine	657/2							
RMS deviations								
Bond length (Å)	0.004							
Bond angles (°)	1.269							

^aPF, Photon Factory, Japan; PAL, Pohang Accelerator Laboratory, Korea.

^bValues in parentheses are for reflections in the highest resolution bin.

^c $R_{\text{merge}} = \frac{\sum_h \sum_i |I(h,i) - \langle I(h) \rangle|}{\sum_h \sum_i I(h,i)}$, where $I(h,i)$ is the intensity of the i^{th} measurement of h and $\langle I(h) \rangle$ is the corresponding average value for all i measurements.

^dFigure of merit = $|\sum P(\alpha)e^{i\alpha} / \sum P(\alpha)|$, where $P(\alpha)$ is the phase probability distribution and α is the phase.

^e R_{work} and $R_{\text{free}} = \frac{\sum ||F_o| - |F_c||}{\sum |F_o|}$ for the working set and test set (5%) of reflections.

The fractions containing MTAN were pooled and human α -thrombin was added at 1 NIH unit/1 mg fusion protein. The GST removed target protein was further purified by anion exchange chromatography (HiTrap Q-Sepharose) followed by gel filtration chromatography (Superose 12). Selenomethionine (SeMet)-substituted MTAN were expressed with B834(DE3) cells and purified as a wild-type protein.

The purified MTAN was concentrated to 10 mg/mL in 50 mM Tris-HCl, pH 8.0, 100 mM NaCl, and 1 mM DTT. Crystallization was performed by the hanging-drop vapor diffusion method at 22°C. A monoclinic crystal form of MTAN was obtained with a reservoir solution consisting of 100 mM Tris-HCl, pH = 8.5, 30% (w/v) polyethylene glycol 4000, and 200 mM sodium acetate. Crystals grew to a maximum size of $0.5 \times 0.3 \times 0.2$ mm³ within 2 days. The native diffraction data were collected on a charge-coupled device detector at the NW12 beamline of the Photon Factory, Tsukuba, Japan. The multiwavelength anomalous dispersion (MAD) data using mercury- and SeMet-derivatives were collected on a charge-coupled device detector at the 4A beamline of the Pohang Accelerator Laboratory, Pohang, Korea. All diffraction data were processed and scaled using the

HKL2000 software package.¹² Statistics for the data collection are described in Table I.

Eight selenium and two mercury sites in the asymmetric unit were located with SOLVE.¹³ The phases were improved with RESOLVE.¹⁴ Statistics for the phasing are presented in Table I. The electron density was of sufficient quality to build a nearly complete model of MTAN with the guidance of EcMTAN coordinates (PDB ID: 1Z5P).¹⁵ The protein model was refined with CNS including the bulk solvent correction.¹⁶ A twofold non-crystallographic symmetry was maintained with tight restraint during the early stages of refinement and was relaxed in the final rounds. Solvent molecules were added using model-phased difference Fourier maps.¹⁶ An unambiguous electron density of adenine was visible, even in the initial MAD-phased map, although the MTAN crystals were obtained in the absence of adenine. Statistics for the refined structures are also presented in Table I. The assessment of model geometry and the assignment of secondary structural elements were obtained by using the program PROCHECK.¹⁷ The AdoHcy model was obtained from the protein data bank (PDB ID: 1HNN) and models of EcMTAN and AtMTAN in complex with AdoHcy were generated by optimal fit-

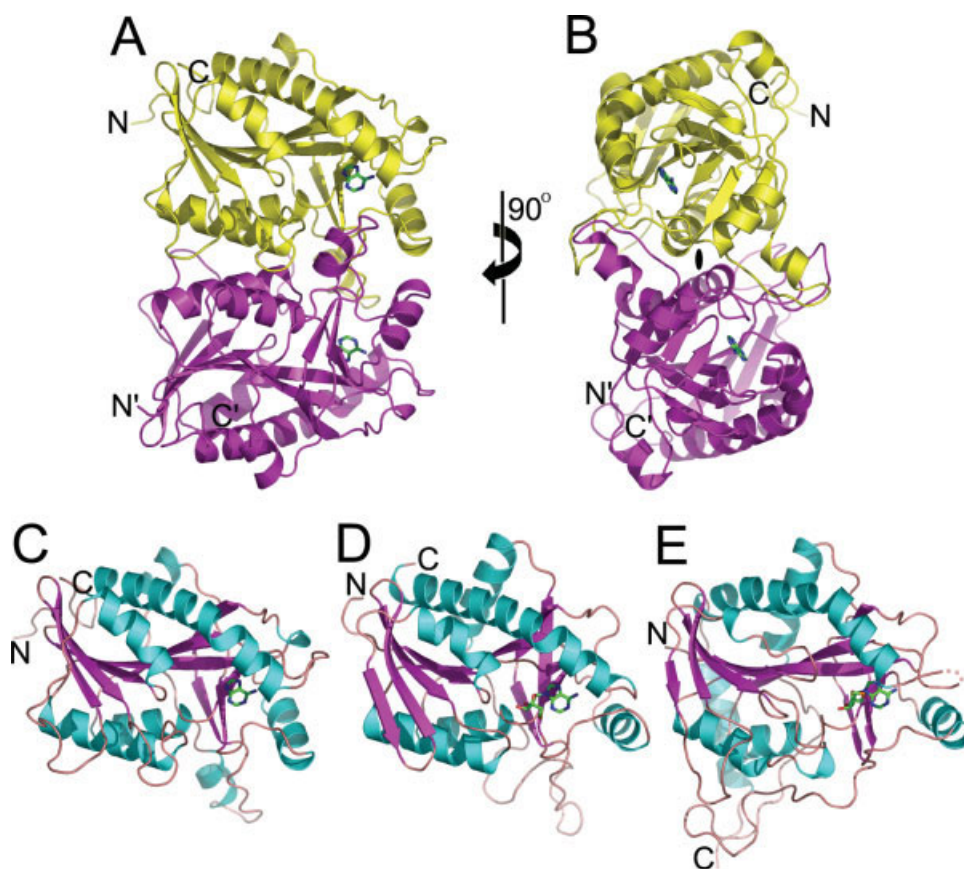


Fig. 1. Overall structure of the AtMTAN and structural comparison. (A) Ribbon diagram showing the dimeric AtMTAN structure and (B) a view along the noncrystallographic twofold molecular symmetry axis. Each monomer in AtMTAN is colored yellow and magenta, respectively. The bound adenine molecules are shown in the stick model. The N- and C-termini of AtMTAN are labeled. (C, D, and E) Structural comparisons among AtMTAN monomer (C), EcMTAN (D), and HsMTAP (E). The view is almost the same as presented in panel A. The α -helices are colored cyan, and the β -sheets and connecting loops are colored magenta and salmon, respectively.

ting into the active sites. All figures were drawn using PyMOL (<http://www.pymol.org>).

Results and Discussion. AtMTAN shares only 25% of sequence identity ($\sim 43\%$ similarity) with EcMTAN and, however, shows significant sequence conservation for the key residues involved in enzymatic catalysis.⁸ The MTAN activity of purified enzyme was confirmed by an assay using radioactive MTA (Oh et al., unpublished results). The oligomeric state of AtMTAN in solution was confirmed as a dimer during the gel filtration step and the dimer was shown to be in the asymmetric unit of present monoclinic crystal form. The crystals diffracted to ~ 2.0 -Å resolution using a laboratory X-ray and up to 1.5-Å resolution using a Synchrotron source. The molecular replacement method was first tried using EcMTAN (PDB ID: 1Z5P), but it failed to yield a solution. Heavy metals were screened for multiple isomorphous replacement phasing and simultaneously SeMet-derivatized proteins were prepared. The structure was phased by multiple wavelength anomalous disper-

sion methods using mercury- and SeMet-derivatives (Table I).

The crystal structure of AtMTAN has been refined at 1.5-Å resolution (Table I). Each monomer of the AtMTAN dimer consisted of seven α -helices, ten β -strands, and two 3_{10} -helices [Fig. 1(C)]. The first 21 residues (Met1-Glu21) of AtMTAN were not observed in the electron density and, therefore, are likely unstructured. The location of bound adenine is in the deep pocket formed by a monomer and the entrance is partially covered by the adjacent subunit [Fig. 1(A)]. This flap is important for forming a wide dimeric interface [Fig. 1(B)]. Structural similarities of AtMTAN with EcMTAN and human MTAP (HsMTAP) are anticipated on the basis of sequence homology, the utilization of the same substrate (MTA) or a combination of the two. The Z-scores by DALI server for EcMTAN and HsMTAP structures are over 20 and 15, respectively, suggesting that they share a notable structural resemblance [Fig. 1(C-E)].¹⁸

AtMTAN and EcMTAN are well superimposed and many active site residues are invariant [Fig. 2(A,B)]. When the adenine binding sites of AtMTAN and EcMTAN are com-

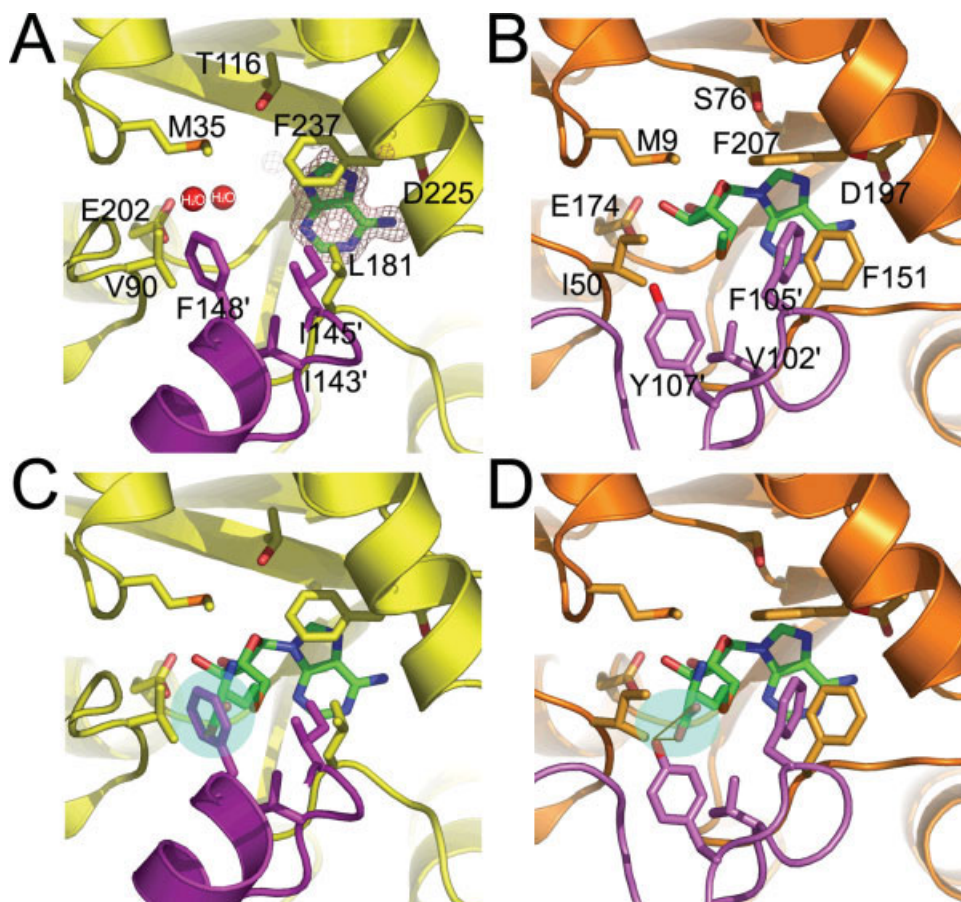


Fig. 2. Close-up view showing the details of the active site in AtMTAN and EcMTAN. (A) A view of the substrate binding site and the electron density map indicating bound adenine in AtMTAN. The $|F_o - F_c|$ map (salmon color) was calculated prior to inclusion of the illustrated adenine molecule in the model. This map was calculated using 50.0–1.5 Å data and was contoured at 3.0σ . (B) The active site of EcMTAN complexed with the substrate (MTA). (C) The active site of AtMTAN; (D) the active site of EcMTAN in complex with AdoHcy. Each subunit covering almost all of the key residues is colored yellow for AtMTAN and orange for EcMTAN, and the other subunit colored magenta for AtMTAN and pink for EcMTAN. Key residues are labeled in the panels A and B. A transparent circle with green coloring represents a steric clash between the phenolic ring of protein and the carboxylic group of homocysteine (C) and that in panel D represents favorable hydrogen bonding interactions between hydroxyl group of the tyrosine residue and the carboxylic group of homocysteine.

pared, the residues are well conserved. The adenine molecule, a reaction product is very clearly defined in 1.5-Å resolution map [Fig. 2(A)]. The carboxylic side chain of Asp225 (D197e; “e” has been attached to represent the residue number of EcMTAN) makes hydrogen bonds with nitrogen atoms in the adenine ring and, therefore, it is a key determinant for the adenine base. Two hydrophobic side chains, Phe237 (Phe207e) and Leu181 (Phe151e) show some structural perturbation to tightly accommodate the adenine ring [Fig. 2(A,B)]. Backbone of Gly118 (Gly78e) also interacts with this region. AtMTAN model in complex with MTA has been generated easily, because the residues recognizing sugar moiety is even more structurally preserved than those recognizing base moiety [Fig. 2(A,B)]. The carboxylic side chain of Glu202 (Glu174e) locates in nearly the same position and two water molecules in the adenine-complex AtMTAN occupy

similar sites where the 2'- and 3'-hydroxyl groups are in sugar moiety in the EcMTAN structure [Fig. 2(A)].

Interesting features can be derived from the AdoHcy model when fitted into the active site of AtMTAN and EcMTAN [Fig. 2(C,D)]. For example, residues Met35 (Met9e), Val90 (Ile50), Ile143' (Val102'e; for clarity we use “prime (’)” to designate residue in one of the two subunits), Ile145' (Phe105'e) make van der Waals contacts with the 5'-alkylthio moiety using their hydrophobic nature. The Ile143' (Val102'e) and Ile145' (Phe105'e) are from a different subunit which cooperates to construct the substrate binding site [Fig. 1(A)]. In EcMTAN, the hydroxyl group of Tyr107'e is able to make hydrogen bonds with the carboxylate group of the homocysteine moiety [Fig. 2(D)]. Basically, there are large conformation differences in the segment of neighboring subunits recognizing the 5'-alkylthio moiety between the bacterial

and plant enzymes. The secondary structural element containing this segment from neighboring subunit is loop in *E. coli* and might be much more flexible than α -helical segment in plant [Fig. 2(C)]. The potential key residue for discriminating AdoHcy, Tyr107^e in the loop region is not able to exactly match the residue in AtMTAN. Because of this helix from the neighboring subunit, the 5'-alkylthio binding site is likely to be limited in plant MTAN than in bacterial MTAN. A protruding bulky side chain of Phe148' shows a clear steric clash but only with the carboxylic end of the homocysteine moiety which is readily interpreted to be that the plant MTAN is able to hydrolyze 5'-methyl, 5'-ethyl, 5'-*n*-butyl, and 5'-isobutylthioadenosine but not AdoHcy.¹⁰

In summary, we present the first MTAN structure from a plant species at very high resolution complexed with a product (adenine) and through a structural comparison with the *E. coli* enzyme provide a clear demonstration of how a plant enzyme cannot hydrolyze AdoHcy in contrast to its bacterial equivalent.

Acknowledgments. We thank the staff at 4A beamline, Pohang Light Source, Korea and NW12 beamline, Photon Factory, Japan for help with the data collection for this study. The atomic coordinates and structure factors (codes 2H8G) have been deposited in the Protein Data Bank (<http://www.rcsb.org>).

REFERENCES

- Schlenk F. Methylthioadenosine. *Adv Enzymol Relat Areas Mol Biol* 1983;54:195–265.
- Sekowska A, Danchin A. The methionine salvage pathway in *Bacillus subtilis*. *BMC Microbiol* 2002;2:8.
- Avila MA, Garcia-Trevijano ER, Lu SC, Corrales FJ, Mato JM. Methylthioadenosine. *Int J Biochem Cell Biol* 2004;6:2125–2130.
- Miyazaki JH, Yang SF. The methionine salvage pathways in relation to ethylene and polyamine biosynthesis. *Physiol Plant* 1987;69:366–370.
- Sauter M, Cornell KA, Beszteri S, Rzewuski G. Functional analysis of methylthioribose kinase genes in plants. *Plant Physiol* 2004;136:4061–4071.
- Yoon SO, Lee YS, Lee SH, Cho YD. Polyamine synthesis in plants: isolation and characterization of spermidine synthase from soybean (*Glycine max*) axes. *Biochim Biophys Acta* 2000;1475:17–26.
- Good X, Kellogg JA, Wagoner W, Langhoff D, Matsumura W, Bestwick RK. Reduced ethylene synthesis by transgenic tomatoes expressing *S*-adenosylmethionine hydrolase. *Plant Mol Biol* 1994;26:781–790.
- Lee JE, Settembre EC, Cornell KA, Riscoe MK, Sufrin JR, Ealick SE, Howell PL. Structural comparison of MTA phosphorylase and MTA/AdoHcy nucleosidase explains substrate preferences and identifies regions exploitable for inhibitor design. *Biochemistry* 2004;43:5159–5169.
- Dunn SM, Bryant JA, Kerr MW. A simple spectrophotometric assay for plant 5'-deoxy-5'-methylthioadenosine nucleosidase using xanthine oxidase as a coupling enzyme. *Phytochem Anal* 1994;26:286–290.
- Guranowski AB, Chiang PK, Cantoni GL. 5'-Methylthioadenosine nucleosidase. Purification and characterization of the enzyme from *Lupinus luteus* seeds. *Eur J Biochem* 1981;114: 293–299.
- Lee JE, Smith GD, Horvatin C, Huang DJ, Cornell KA, Riscoe MK, Howell PL. Structural snapshots of MTA/AdoHcy nucleosidase along the reaction coordinate provide insights into enzyme and nucleoside flexibility during catalysis. *J Mol Biol* 2005;352: 559–574.
- Otwinowski Z, Minor W. Processing of X-ray diffraction data collected in oscillation mode. In: Carter CW Jr, Sweet RM, editors. *Methods enzymol*, Vol. 276. New York: Academic Press; 1997. pp 307–326.
- Terwilliger TC, Berendzen J. Automated MAD and MIR structure solution. *Acta Crystallogr Sect D* 1999;55 (Part 4):849–861.
- Terwilliger TC. Automated main-chain model building by template matching and iterative fragment extension. *Acta Crystallogr Sect D* 2003;59 (Part 1):38–44.
- Jones TA, Zou J-Y, Cowan SW, Kjeldgaard M. Improved methods for binding protein models in electron density maps and the location of errors in these models. *Acta Crystallogr Sect A* 1991;47 (Part 2):110–119.
- Brunger AT, Adams PD, Clore GM, DeLano WL, Gros P, Grosse-Kunstleve RW, Jiang JS, Kuszewski J, Nilges M, Pannu NS, Read RJ, Rice LM, Simonson T, Warren GL. Crystallography & NMR system: a new software suite for macromolecular structure determination. *Acta Crystallogr Sect D* 1998;54 (Part 5): 905–921.
- Laskowski R, MacArthur M, Hutchinson E, Thornton J. PROCHECK: a program to check the stereochemical quality of protein structures. *J Appl Crystallogr* 1993;26:283–291.
- Holm L, Sander C. Protein structure comparison by alignment of distance matrices. *J Mol Biol* 1993;233:123–138.